

Jet spectroscopy and excited state dynamics of SiH₂ and SiD₂

Masaru Fukushima, Shinya Mayama, and Kinichi Obi

Citation: *The Journal of Chemical Physics* **96**, 44 (1992); doi: 10.1063/1.462479

View online: <http://dx.doi.org/10.1063/1.462479>

View Table of Contents: <http://scitation.aip.org/content/aip/journal/jcp/96/1?ver=pdfcov>

Published by the [AIP Publishing](#)

Articles you may be interested in

[Cavity ring-down spectroscopy of jet-cooled silane isotopologues in the Si–H stretch overtone region](#)

J. Chem. Phys. **127**, 244301 (2007); 10.1063/1.2819072

[An accurate description of the ground and excited states of SiH](#)

J. Chem. Phys. **116**, 6529 (2002); 10.1063/1.1461817

[Strong isotope effects in the dissociation kinetics of Si–H and Si–D complexes in GaAs under ultraviolet illumination](#)

Appl. Phys. Lett. **75**, 112 (1999); 10.1063/1.124292

[Vibrational dynamics of the Si–H stretching modes of the Si\(100\)/H:2×1 surface](#)

J. Chem. Phys. **102**, 4269 (1995); 10.1063/1.469474

[Lifetimes and Total Transition Probabilities for NH, SiH, and SiD](#)

J. Chem. Phys. **51**, 520 (1969); 10.1063/1.1672027



Jet spectroscopy and excited state dynamics of SiH₂ and SiD₂

Masaru Fukushima, Shinya Mayama, and Kinichi Obi

Department of Chemistry, Tokyo Institute of Technology, Ohokayama, Meguro, Tokyo 152, Japan

(Received 14 March 1991; accepted 18 September 1991)

Silylene radicals, SiH₂ and SiD₂, are generated in a supersonic free jet by ArF laser (193 nm) photolysis of phenylsilane and phenylsilane-*α*-d₃, respectively. LIF excitation and dispersed fluorescence spectra are measured for the ν_2 vibronic bands of the $\tilde{A}^1B_1 - \tilde{X}^1A_1$ transition. The heterogeneous predissociation to Si(³P) + H₂ is proposed from the anomalous rotational structure in the excitation spectra; the rotational lines of the $r(1)$ subbranch ($K'_a = 0 - K''_a = 1$) have stronger intensity than those of the $r(0)$ subbranch ($K'_a = 1 - K''_a = 0$), though the latter is expected to be stronger due to the low temperature Boltzmann distribution in the jet. The time-resolved excitation spectra demonstrate shorter lifetime of $K'_a = 1$ rovibronic levels in the \tilde{A}^1B_1 state. The heterogeneous predissociation is interpreted with the second order perturbation: $\tilde{A}^1B_1 - (a\text{-type Coriolis}) \rightarrow \tilde{X}^1A_1 - (\text{spin-orbit}) \rightarrow \tilde{a}^3B_1 \rightarrow \text{Si}(\text{}^3P) + \text{H}_2$. It is demonstrated experimentally that there is a potential barrier associated with the dissociation path of $\tilde{a}^3B_1 \rightarrow \text{Si}(\text{}^3P) + \text{H}_2$, the height of which is estimated to be 1540–2160 cm⁻¹ from the bottom of the \tilde{A}^1B_1 state. The electronic transition moment of the $\tilde{A}^1B_1 - \tilde{X}^1A_1$ transition is estimated to be $|\mu_e|^2 = 0.26e^2a_0^2$ from the Einstein equation for spontaneous emission using measured fluorescence lifetimes for single rovibronic levels with $K'_a = 0$ and calculated Franck–Condon factors. The onset of a second predissociation channel, $\tilde{A}^1B_1 \rightarrow \text{Si}(\text{}^1D) + \text{H}_2$, at the (0,7,0) vibronic level of SiH₂ \tilde{A}^1B_1 is manifested as a sharp decrease in the observed fluorescence lifetime for the $\nu'_2 = 7, J' = 0$ level relative to that predicted for a pure radiative lifetime.

I. INTRODUCTION

The silylene radical (SiH₂) is one of the simplest polyatomic molecules containing silicon. Recently much interest has focused on the nature of its reactivity due to profitable applications of silicon-containing materials. However, many of the photophysical and photochemical properties of SiH₂ remain unexplored, despite their potentially important role in reactions involved in the silicon semiconductor manufacturing process. This is in a marked contrast to the extensive spectroscopic and dynamical investigations on the CH₂ radical, a molecule isovalent with SiH₂.

Absorption spectra of the SiH₂ radical were first observed in the flash photolysis of silane or phenylsilane.¹ A highly structured band system was attributed to the *c*-type transition between the \tilde{X}^1A_1 and \tilde{A}^1B_1 states generated from the ¹Δ state in the linear configuration under the Renner–Teller interaction. Dubois *et al.*¹ reported the rotational constants and vibrational frequencies of the bending mode and suggested that the rotational structure of high vibronic levels in the \tilde{A} state was not expressible in terms of a simple rotational Hamiltonian because of the strong Renner–Teller interaction and a large amplitude bending vibration. From rotational analysis of several vibronic bands, a barrier height to the linear configuration in the \tilde{A} state was estimated to be ~8000 cm⁻¹. The frequencies of the bending mode (ν_2) and the H–Si–H bond angles were determined to be 1004 cm⁻¹ and 92.08° for \tilde{X}^1A_1 , and 860 cm⁻¹ and 123° for the \tilde{A}^1B_1 states, respectively. The large change in bond angle upon electronic excitation is responsible for the long progression in the bending mode. Milligan and Jacox² and Fre-

din *et al.*³ determined the frequencies of all three fundamentals in the \tilde{X}^1A_1 state from matrix isolation spectra: 1964, 995, and 1993 cm⁻¹ for ν_1 , ν_2 , and ν_3 , respectively.³

Theoretical calculations of ground and excited state geometries and vibrational frequencies are also available.^{4–9} Potential surfaces of low lying electronic states have been calculated and the excited state dynamics have been discussed.⁶

Fluorescence excitation spectra of the $\tilde{A} - \tilde{X}$ transition and fluorescence lifetimes of the \tilde{A}^1B_1 state have been measured by Inoue and Suzuki.¹⁰ Fluorescence lifetimes were reported as being ~60 ns, in contrast to the much longer lifetimes observed for the \tilde{b}^1B_1 state of the isovalent radical, CH₂, 4.2 μs.¹¹ Steinfeld and co-workers,¹² and Francisco *et al.*¹³ have measured fluorescence lifetimes for a large number of rovibronic levels in the \tilde{A}^1B_1 state of SiH₂. They observed wide variations in lifetimes (< 10 ns to > 1 μs) for neighboring rotational levels in the same vibronic state. The widely varying lifetimes for levels in the \tilde{A}^1B_1 state were interpreted in terms of a model that involved predissociation of SiH₂ to Si(³P) + H₂, as we previously suggested.¹⁴ Very recently, Knight and co-workers^{12(e)} have verified this interpretation with the direct observation of Si(³P) following state-selected excitation of SiH₂.

In this paper, we present a detailed investigation of the spectroscopy and excited state dynamics of SiH₂ and SiD₂ generated in a supersonic free jet expansion. Fluorescence excitation spectra, dispersed fluorescence spectra, and fluorescence lifetimes are measured and the mechanism of predissociation is discussed.

II. EXPERIMENTAL

The apparatus used is the same as that reported previously.¹⁵ A homemade pulsed valve with a 500 μm diam orifice was mounted to a vacuum chamber. The background pressure was $\sim 10^{-6}$ Torr with the valve closed and $\sim 10^{-4}$ Torr during operation with a stagnation pressure of ~ 760 Torr. Silylene radicals, SiH₂ (or SiD₂), were produced by ArF laser photolysis, at the nozzle exit, of phenylsilane, $\phi\text{-SiH}_3$ (or phenylsilane- $\alpha\text{-d}_3$, $\phi\text{-SiD}_3$), seeded in an Ar jet. Laser induced fluorescence (LIF) signals were observed 35 mm downstream ($X/D = 70$) from the orifice using an N₂ laser pumped dye laser intersecting the jet at right angles to the direction of propagation of the gas pulse. The linewidth of the dye laser was $\sim 0.3 \text{ cm}^{-1}$. Absolute wavelength calibration was achieved with the opto-galvanic signal from a Ne hollow cathode tube. Fluorescence was detected with a photomultiplier (Hamamatsu Photonics, R-1477) and amplified by a homemade socket-type preamplifier before input to a gated integrator (NF, BX-531). Time resolved excitation spectra were measured using a 0.25 m monochromator (Nikon, P-250) to reject scattered light from the excitation laser. In this case, signals were enhanced with a wide-band amplifier ($\sim 100 \text{ MHz}$).

Dispersed fluorescence spectra were measured using the 0.25 m monochromator. $\phi\text{-SiH}_3$ was obtained as a commercial reagent (Shin-Etsu Chemical). $\phi\text{-SiD}_3$ was prepared by reduction of $\phi\text{-SiCl}_3$ with LiAlD₄ in dry ether and purified by distillation. $\phi\text{-SiD}_3$ purity was established as $> 99\%$ from NMR and mass spectroscopy.

III. RESULTS

A. LIF excitation spectrum of the SiH₂ $\tilde{A}^1B_1 - \tilde{X}^1A_1$ transition

LIF excitation spectra of eight vibronic bands of the SiH₂ $\tilde{A}^1B_1 - \tilde{X}^1A_1$ transition were measured in the wavelength region 460–640 nm under jet conditions. The spectra obtained for $v_2' = 0$ to 5 are shown in Fig. 1. Vibrational assignments follow those established from the absorption spectrum at room temperature.¹

Rotational structure conforms with that expected for perpendicular bands of a c -type transition for which the selection rules are given by¹⁶

$$\Delta J = 0, \pm 1, \quad \Delta K_a = \pm 1, \pm 3, \quad \text{and} \quad \Delta K_c = 0, \pm 2.$$

Figure 2 illustrates the allowed transitions for low rotational levels. Dubois *et al.* determined rotational constants for the $v_2' = 0\text{--}3$ vibronic levels of the \tilde{A}^1B_1 state from high J values. Our line positions for low J values were estimated using their rotational constants and our assignments are shown in Fig. 1. We note that lines corresponding to the r subband, which are expected to be strong under jet conditions, were almost absent in our spectra. A similar observation was reported by Steinfeld and co-workers.¹² Several lines appeared to be unassignable in our spectra. These may result from perturbations or may have escaped assignment simply because molecular constants deduced from high J values were used to analyze low J lines. The strongest lines observed in other vibronic bands were attributed to $^pP_1(1)$ by analogy

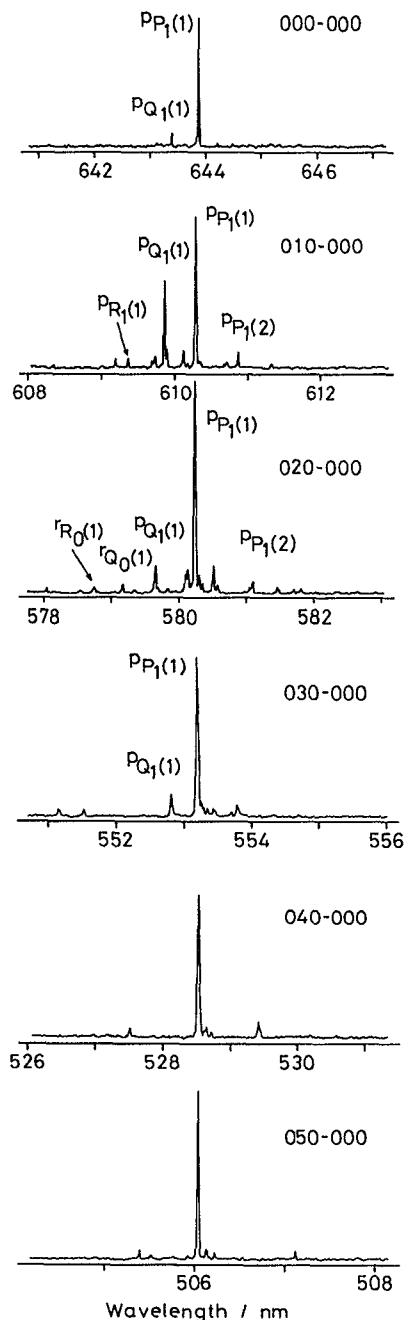


FIG. 1. LIF excitation spectra of the SiH₂ $\tilde{A}^1B_1(0, v_2', 0) - \tilde{X}^1A_1(0, 0, 0)$, $v_2' = 0\text{--}5$ transition. Signals are integrated for 0–5 μs .

with the above observations though no detailed rotational analysis is reported here for these bands. An anomaly is seen in the line intensity of $^pQ_1(1)$, which had been expected to be stronger than $^pP_1(1)$ from our line intensity calculation. The observed line intensity of $^pQ_1(1)$ is found to be much weaker than that of $^pP_1(1)$ and decreases with increasing bending vibrational quantum number. These intensity anomalies in the excitation spectra are consistent with the proposal of rotational level-dependent nonradiative processes,^{12(b),14} since similar anomalies were not observed in the absorption spectrum.¹

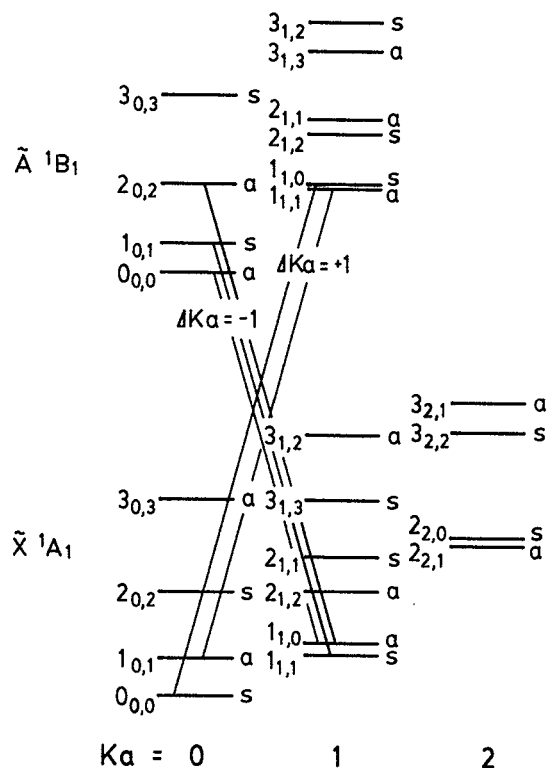


FIG. 2. Rotational levels of the \tilde{A}^1B_1 and \tilde{X}^1A_1 states and allowed transitions of SiH₂.

To further quantify the rotational dependence of this nonradiative process in the \tilde{A} state, time resolved LIF excitation spectra were measured for eight vibronic bands. Figures 3 and 4 show those of the $(0, v_2', 0) - (0, 0, 0)$, $v_2' = 2$ and 6, bands. These spectra indicate that the lifetime of rotational levels is strongly dependent on rotational quanta, J and K_a . The $r(0)$ subbranch for $(0, 2, 0) - (0, 0, 0)$ terminating at the levels of $K_a' = 1$ was observed in the early stage (0–50 ns), but not in the late (50–100 ns), although the $p(1)$ subbranch had almost the same strength in both time stages. The $r(0)$ subbranch was observed up to $v_2' = 5$ in the early-time spectra, but its intensity decreased with increasing vibrational quanta.

The $(0, 6, 0)$ level showed anomalous behavior. Since the rotational assignment of the $(0, 6, 0) - (0, 0, 0)$ band has not been reported, we attempted to analyze the rotational structure using rotational constants derived from the analysis of lower vibrational levels. Tentative assignments are shown in Fig. 4 although calculated line strengths were not consistent with the observed line intensities in the spectrum. It is noteworthy that the $^pQ_1(1)$ and $^pR_1(1)$ lines, which are weak and short lived in other bands, appear with significant intensity in the $(0, 6, 0) - (0, 0, 0)$ band and survive with a lifetime of 30 ns.

The line positions of the strongest rotational lines, $^pP_1(1)$, observed for the eight vibronic bands are listed in Table I. From the line positions in Table I, the vibrational frequency of the bending mode, ω_2' , in the \tilde{A} state of SiH₂ was determined as shown in Table II. Our value, $\omega_2' = 850$

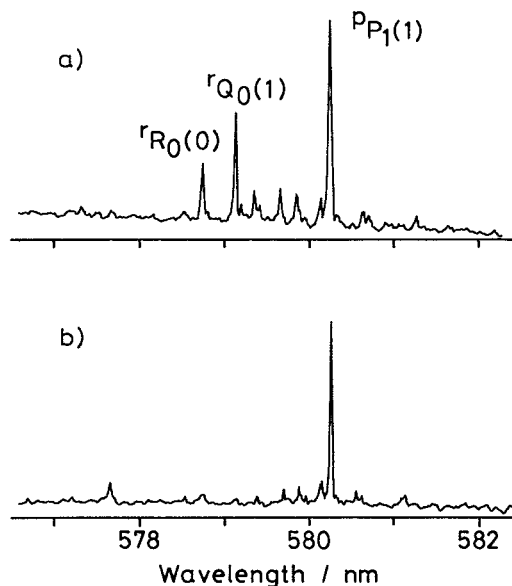


FIG. 3. Time resolved excitation spectra of the SiH₂ $\tilde{A}^1B_1(0,2,0) - \tilde{X}^1A_1(0,0,0)$ transition. (a) Detection gate was open between 0 and 50 ns after dye laser excitation. (b) Detection gate was open between 50 and 100 ns.

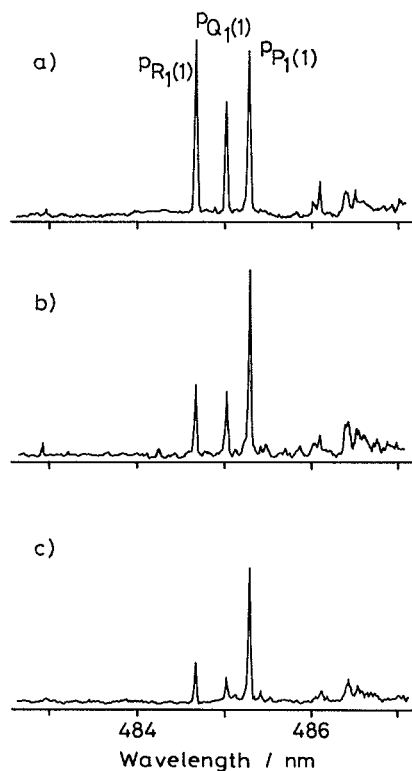


FIG. 4. Time resolved excitation spectra of the SiH₂ $\tilde{A}^1B_1(0,6,0) - \tilde{X}^1A_1(0,0,0)$ transition. (a) Detection gate was open between 0 and 50 ns after dye laser excitation. (b) Detection gate was open between 50 and 100 ns. (c) Detection gate was open between 100 and 150 ns.

TABLE I. Vacuum wave numbers and vibrational assignments of vibronic bands [^pP₁(1)] of SiH₂.

v_2'	v_2''	Vibronic band (cm ⁻¹)
0	0	15 531
1	0	16 384
2	0	17 233
3	0	18 077
4	0	18 919
5	0	19 761
6	0	20 605
7	0	21 453

cm⁻¹, shows good agreement with 860 cm⁻¹ reported by Dubois *et al.*¹

B. LIF excitation spectrum of the SiD₂ $\tilde{A}^1B_1 - \tilde{X}^1A_1$ transition

LIF excitation spectra were measured for 11 vibronic bands of the SiD₂ $\tilde{A}^1B_1 - \tilde{X}^1A_1$ transition in the wavelength region 460–640 nm. Vibrational assignments follow those established from the absorption spectra.¹ The spectra obtained for $v_2' = 0$ to 5 are shown in Fig. 5. Rotational assignments for the $\tilde{A} - \tilde{X}$ transition in SiD₂ are not previously available. Rotational assignments shown in Fig. 5 are based on rotational analysis of high resolution spectra¹⁷ measured using an intracavity etalon in the dye laser. LIF excitation spectra of SiD₂ shown in Fig. 5 display more complicated rotational structure than that observed in SiH₂. The rotational structure becomes simpler in bands terminating at higher vibronic levels, as is the case for SiH₂. In contrast to SiH₂, *r* subbands observed for SiD₂ display appreciable intensity in the low vibronic bands ($v_2' = 0, 1, \text{ and } 2$). However, for vibronic bands involving $v_2' \geq 3$, only *p* subbands were observed.

Figure 6 shows time resolved LIF excitation spectra of the (0,2,0)–(0,0,0) vibronic band in SiD₂. The time dependence of the *r* subbands is seen to be similar to that observed in SiH₂. As may be seen in Fig. 6, *r* subbands terminating at $K_a \neq 0$ display strong intensity in the spectrum obtained at early times, but disappear at later times.

TABLE II. Vibrational constants (cm⁻¹) of the v_2 bending mode.

	SiH ₂		SiD ₂		
	\tilde{A}	\tilde{X}	\tilde{A}	\tilde{X}	
ω_2	850	1009	616	731	This work
	860	1004	610		In gas phase ^a
		995		720	In Ar matrix ^b
x_{22}		-4.3		-2.7	This work

^aReference 1.

^bReference 3.

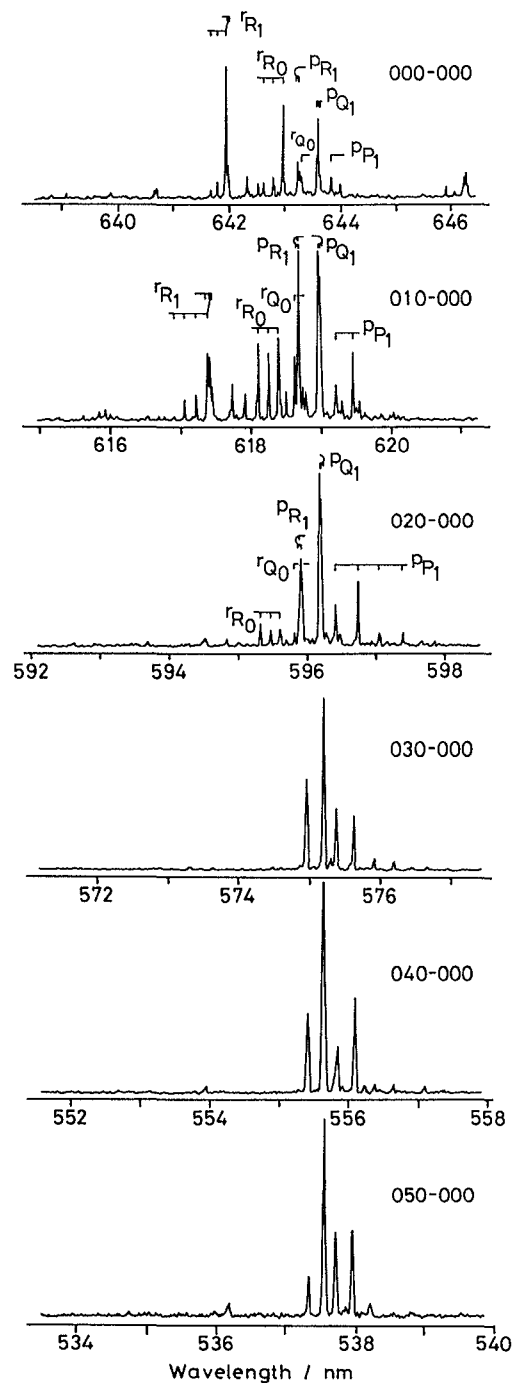


FIG. 5. LIF excitation spectra of the SiD₂ $\tilde{A}^1B_1(0, v_2', 0) - \tilde{X}^1A_1(0, 0, 0)$, $v_2' = 0-5$ transition. Signals are integrated for 0–5 μ s.

The line positions of the strongest rotational lines, ^pP₁(1), observed for the 13 vibronic bands are listed in Table III. From the line positions with $v_2'' = 0$ in Table III, the vibrational frequency of the bending mode, ω_2' , in the \tilde{A} state of SiD₂ was determined as shown in Table II. Our value, $\omega_2' = 616$ cm⁻¹, shows good agreement with 610 cm⁻¹ reported by Dubois *et al.*¹

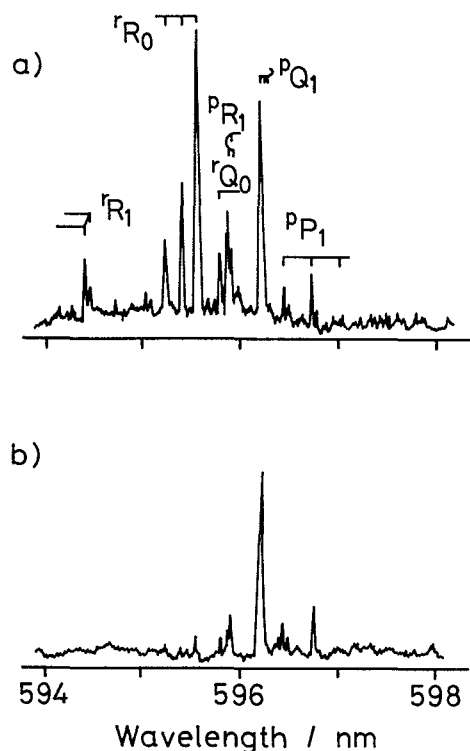


FIG. 6. Time resolved excitation spectra of the SiD₂ $\tilde{A}^1B_1(0,2,0) - \tilde{X}^1A_1(0,0,0)$ transition. (a) Detection gate was open between 0 and 50 ns after dye laser excitation. (b) Detection gate was open between 50 and 100 ns.

C. Dispersed fluorescence spectra and Franck-Condon factors

Dispersed fluorescence spectra were obtained following excitation to vibronic levels, $v_2' = 1 \sim 7$ of SiH₂ and $v_2' = 1 \sim 8$ of SiD₂ in the \tilde{A}^1B_1 state. Spectra from $v_2' = 0$ of SiH₂ and $v_2' = 0, 9$, and 10 of SiD₂ could not be obtained because of insufficient intensity. Examples of dispersed spectra are

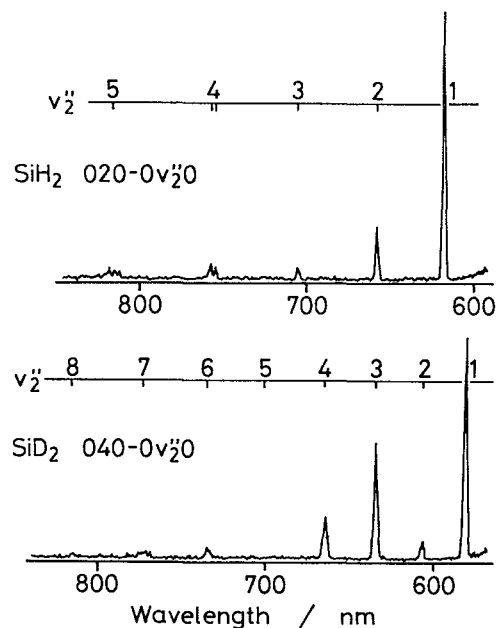


FIG. 7. Dispersed fluorescence spectra obtained following excitation of SiH₂(0,2,0) and SiD₂(0,4,0) in the \tilde{A}^1B_1 state.

shown in Fig. 7 for (0,2,0) excitation of SiH₂ and for (0,4,0) excitation of SiD₂. The observed spectra consist of a single dominant vibrational progression involving an interval of $\sim 1000 \text{ cm}^{-1}$ for SiH₂ and $\sim 700 \text{ cm}^{-1}$ for SiD₂, which may be assigned to the bending mode, ν_2 , based on vibrational frequencies measured in an Ar matrix.³ Deslandres tables of SiH₂ and SiD₂ were constructed from the observed line positions as shown in Tables IV and V, respectively. Vibrational constants were obtained from these tables by considering a single anharmonicity term x_{22} , and the results are listed in Table II. Values obtained for ω_2 are in good agreement with those reported in previous gas phase¹ and Ar matrix studies.³ The anharmonicities in the excited state were too small to be estimated due to our limited experimental resolution.

The emission bands of SiH₂ terminating at $v_2'' = 4$ ap-

TABLE III. Vacuum wave numbers and vibrational assignments of vibronic bands [$^pP_1(1)$] of SiD₂.

v_2'	v_2''	Vibronic band (cm ⁻¹)
0	0	15 545
1	0	16 163
2	0	16 773
3	0	17 385
4	0	17 996
5	0	18 603
6	0	19 201
7	0	19 803
8	0	20 401
9	0	20 998
10	0	21 599
1	1	15 439
2	2	15 336

TABLE IV. Deslandres table (cm⁻¹) for dispersed fluorescence spectra of SiH₂ (emitting levels $v_2' = 1 \sim 7$).

$v_2' \setminus v_2''$	0	1	2	3	4	5	6
0							
1	16 384	15 320	14 334	13 358			
2	17 233	16 165	15 188	14 158	13 243	12 285	
3	18 077	17 090	16 066	15 094	14 150	13 194	
4	18 919		16 845	15 857	14 086		
5	19 761	18 668	17 682		13 976*	12 988	
6	20 605	19 527	18 509	17 543	15 762	14 721	
7	21 453	20 378	19 391	18 377	15 691	14 641	16 438

*Splitting due to Fermi resonance in the ground state.

TABLE V. Deslandres table (cm⁻¹) for dispersed fluorescence spectra of SiD₂ (emitting levels $v_2' = 1-8$).

$v_2' \setminus v_2''$	0	1	2	3	4	5	6	7	8
0									
1	16 163	15 322	14 597	13 891	13 194	12 498			
2	16 773	15 946	15 228	14 521		13 085	12 362		
3	17 385	16 560	15 848	15 106	14 403	13 706	12 998		
4	17 996	17 170	16 438	15 720	15 013		13 584	12 903	12 227
5	18 603	17 776	17 044	16 333		14 916	14 208		12 840
6	19 201		17 659	16 940	16 216	15 515			
7	19 803	18 961	18 240		16 820				
8	20 401	19 586	18 860	18 141	17 410	16 724	16 003		

pear as doublets with an observed splitting of ~ 50 cm⁻¹ in all spectra. This splitting is presumably due to Fermi resonance between $4\nu_2$ and either $2\nu_1$ or $2\nu_3$. Fermi resonance was reported between $2\nu_2$ and ν_1 in the IR spectra of SiH₂ and SiD₂ in an Ar matrix.³ Under our experimental conditions, Fermi resonance does not appear at $2\nu_2$, presumably because of differences in vibrational frequencies between the matrix and the gas phase.

Low vibrational levels of \tilde{X}^1A_1 and \tilde{A}^1B_1 are found to be fairly harmonic, e.g., the anharmonic constant, x_{22}'' , is estimated as -4.3 cm⁻¹, which is small compared with that for methylene,¹⁸ -18.2 cm⁻¹. Hence, Franck-Condon factors were calculated using a harmonic oscillator model.¹⁹ Observed intensities for bands terminating at $v_2'' = 4$ were taken as the sum of intensities for the two members of the Fermi doublet. The molecular constants used for the calculation were as follows. The values determined in this work were used for the vibrational frequencies of ν_2 . The geometrical parameters for SiH₂ were as reported previously¹ and those for SiD₂ were derived from high resolution spectra of the $\tilde{A}-\tilde{X}$ transition.¹⁷ Values chosen for ν_1 and ν_3 in the \tilde{X} state for both radicals were those observed in an Ar matrix,³ while for the SiH₂ \tilde{A} state, values chosen were as calculated by Colvin *et al.*,⁵ since there are no experimental estimates available. For the SiD₂ \tilde{A} state, ν_1 and ν_3 were estimated using the approximation, $\nu_n'(\text{SiD}_2) = \nu_n'(\text{SiH}_2)/\sqrt{2}$. The relative band intensities estimated from Franck-Condon factors calculated using these data are illustrated in Figs. 8 and 9 together with observed intensities. The calculated intensities match well with those observed in the emission spectra.

D. Fluorescence lifetimes for the \tilde{A}^1B_1 state

Fluorescence lifetimes for $J' = 0, K_a' = 0, K_c' = 0$ rovibronic levels of the \tilde{A}^1B_1 state were measured for several vibrational levels, namely $v_2' = 0-7$ for SiH₂ and $v_2' = 0-10$ for SiD₂. The $^3P_1(1)$ rovibronic transitions are sufficiently strong to yield fairly precise estimates for these $J' = 0$ fluorescence lifetimes. Typical logarithmic plots of the fluorescence decay curves are shown in Fig. 10. Single exponential decays are observed in all cases. The lifetimes are summarized in Table VI. As may be seen from the table, the fluorescence lifetimes for these $0_{0,0}$ rotationless levels tend to de-

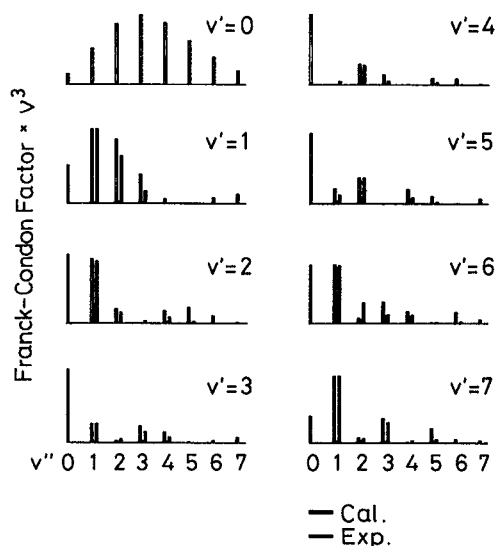


FIG. 8. Calculated Franck-Condon factors (multiplied by the cube of the transition wave number) compared with observed fluorescence intensities for dispersed fluorescence progressions involving ν_2 in SiH₂.

crease from $1.1 \mu\text{s}$ to $0.4 \mu\text{s}$ with an increase in the vibrational excitation energy. Thoman *et al.*^{12(b)} also reported the lifetime of $0_{0,0}, v_2' = 2$ to be $1.0 \mu\text{s}$, in good agreement with our value.

A few fluorescence lifetimes for rotationally excited levels were also measured. Measurements were made only for $(0,1,0)$ and $(0,6,0)$ in SiH₂ and for $(0, v_2', 0)$, $v_2' = 0-7$ in SiD₂. The fluorescence lifetimes are 850 and 60 ns for $(0,1,0)$ and $(0,6,0)$ in SiH₂, respectively. These were found to be generally short. We were not able to measure fluores-

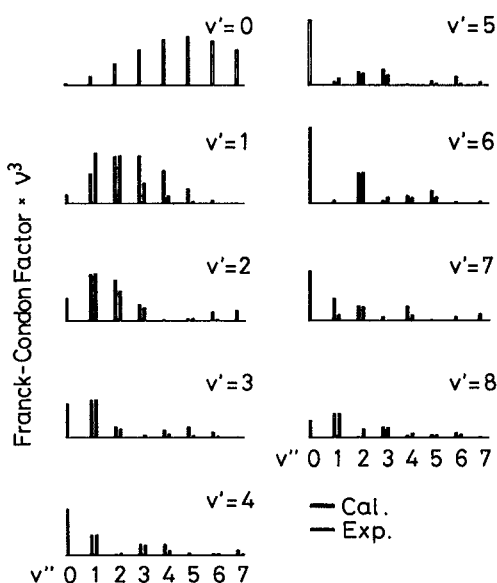


FIG. 9. Calculated Franck-Condon factors (multiplied by the cube of the transition wave number) compared with observed fluorescence intensities for dispersed fluorescence progressions involving ν_2 in SiD₂.

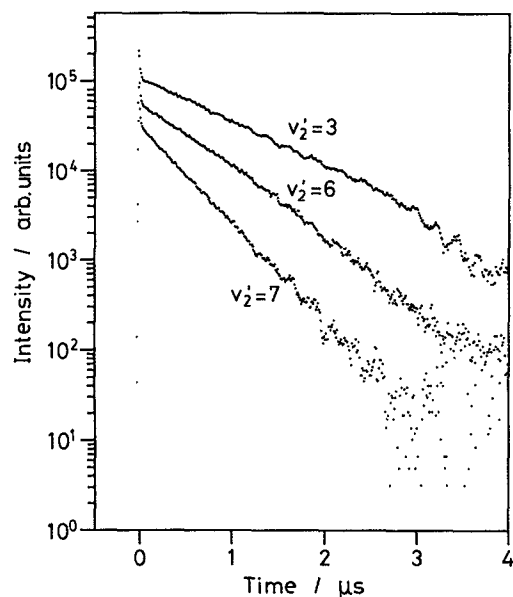


FIG. 10. Time profiles of fluorescence intensity for SiH₂ excited at $P_1(1)$, $v_2' = 3, 6$ and 7 . (The weak oscillation observed on the weak signal region after $3 \mu\text{s}$ for $v_2' = 3$ is apparatus artifacts.)

cence lifetimes for other rotationally excited vibronic levels due to their shortness relative to our experimental time resolution. However, we may estimate an upper limit of ~ 30 ns from the time resolved excitation spectra.

IV. DISCUSSION

A. Radiative lifetime of the \tilde{A}^1B_1 state of silylene

Since intensities for the v_2 progression in the dispersed fluorescence spectra are modelled well by calculated harmonic Franck–Condon factors as illustrated above, the transition moment is assumed to be relatively insensitive to the valence angle, at least up to $v_2' = 7$, $v_2'' = 7$ for SiH₂ and $v_2' = 8$, $v_2'' = 7$ for SiD₂. According to Einstein's treatment, radiative decay rates are proportional to the cubed power of the effective transition energy and may be formulated as follows:

TABLE VI. Fluorescence lifetimes (μs) of $0_{0,0}$ rotationless single rovibronic levels in \tilde{A}^1B_1 .

v_2'	SiH ₂	SiD ₂
0	1.1 ± 0.17	0.93 ± 0.38
1	1.0 ± 0.18	0.92 ± 0.23
2	1.0 ± 0.27	1.1 ± 0.04
3	0.82 ± 0.17	0.86 ± 0.15
4	0.77 ± 0.03	0.80 ± 0.03
5	0.69 ± 0.07	0.66 ± 0.06
6	0.60 ± 0.03	0.72 ± 0.09
7	0.40 ± 0.01	0.67 ± 0.12
8		0.67 ± 0.12
9		0.63 ± 0.11
10		0.63 ± 0.12

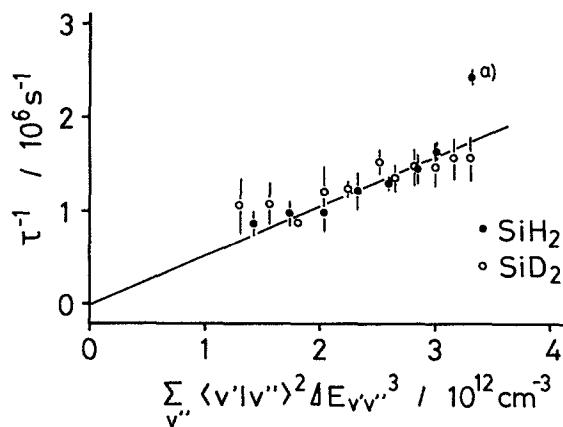


FIG. 11. Fluorescence decay rates for $0_{0,0}$ rovibronic levels in SiH₂ and SiD₂, \tilde{A}^1B_1 state plotted against cubed power of the transition energy. [Eq. (2) in the text] (a) indicates $v_2' = 7$ in SiH₂.

$$k_r = \frac{64\pi^4 \sum_{J',K'} S_{J',K'} d_n}{3h (2J' + 1) d_m} |\mu_e|^2 \sum_{v',v''} |\langle v'|v'' \rangle|^2 \Delta E_{v',v''}^3, \quad (1)$$

where $|\langle v'|v'' \rangle|^2$ is the Franck–Condon factor, $\Delta E_{v',v''}$ is the vibronic transition energy, μ_e is a transition moment, d_n and d_m are degeneracies of the excited and ground states, respectively, and $S_{J',K'}$ is the line strength for each rotational transition. The term $\sum_{J',K'} S_{J',K'} / (2J' + 1)$ is unity from the sum rule, and in our case, d_n and d_m are identical. Hence, for our purposes, Eq. (1) is reduced to

$$k_r = \frac{64\pi^4}{3h} |\mu_e|^2 \sum_{v',v''} |\langle v'|v'' \rangle|^2 \Delta E_{v',v''}^3. \quad (2)$$

Our measured $J' = 0$ fluorescence decay rates, τ^{-1} , which are the sum of radiative and nonradiative rate constants, are plotted in Fig. 11 according to Eq. (2). All the data for $0_{0,0}$ rotational levels of SiH₂ and SiD₂, except that for SiH₂ (0,7,0), conform to a straight line having zero intercept. The electronic transition moment is estimated to be $|\mu_e|^2 = 0.26e^2a_0^2$ from the slope. Since with the exception of the lifetime of the $J' = 0$ level of SiH₂ (0,7,0), there are no deviation from a linear relationship, and the intercept is zero, we may conclude that nonradiative processes are not operative in this system except for SiH₂ (0,7,0). The $J' = 0$ lifetimes reported in Table VI, hence, correspond to pure radiative lifetimes for the \tilde{A}^1B_1 state (with the exception of that for $v_2' \geq 7$ for SiH₂). Koseki and Gordon⁶ calculated the transition moment as a function of normal coordinates, in which the transition moment at the equilibrium configuration in the \tilde{A}^1B_1 state was estimated to be $\mu_e \simeq 0.63ea_0$. Our experimentally determined value displays reasonable agreement, given the precision of the calculated value. The fluorescence lifetime for SiH₂ (0,7,0) is shorter than that expected from spontaneous emission alone. This indicates that a nonradiative decay channel opens at (0,7,0) for SiH₂.

B. Nonradiative processes in the \tilde{A}^1B_1 state

Previous studies^{12–14} indicate that the \tilde{A}^1B_1 state of silylene shows anomalous spectroscopic and photophysical behavior:

(1) Unassignable rotational lines by a standard rotational Hamiltonian in LIF excitation spectra.

(2) Wide variation of fluorescence lifetimes.

(3) Existence of dissociation channels to produce Si (³P) and Si (¹D) + H₂.

Silylene lacks adequate level density for intramolecular non-radiative processes without predissociation, as suggested previously.^{12(b)} We see this also to be the case for the isovalent molecule CH₂ where nonradiative decay of the excited \tilde{b}^1B_1 state does not occur, despite the fact that the \tilde{b}^1B_1 state interacts strongly with the ground state \tilde{X}^3B_1 .²⁰ In the case of silylene, the lowest dissociation limit, Si (³P_J) + H₂ (¹Σ_g⁺), lies lower than the zero point energy of the \tilde{A} state, which was first proposed by our group¹⁴ and later confirmed by Steinfeld and co-workers.¹² The second dissociation limit, Si (¹D) + H₂ (¹Σ_g⁺) also lies within the lower part of the vibronic manifold of the \tilde{A}^1B_1 state, but the next dissociation channel, yielding SiH + H, occurs at a much higher energy.²¹ Theoretical calculation^{5,9} predicted that there are \tilde{a}^3B_1 and 3A_2 states around energy region of the \tilde{A}^1B_1 state. Previous studies¹²⁻¹⁴ explain the anomalous behavior of the \tilde{A}^1B_1 state in terms of interaction of the \tilde{A}^1B_1 state with triplet states, \tilde{a}^3B_1 and 3A_2 states, through which SiH₂ dissociates to Si (³P) + H₂. Steinfeld and co-workers^{12(b),12(d)} proposed a mechanism for Si (³P) production from SiH₂, i.e., extensive random state mixing between the excited \tilde{A}^1B_1 state and other low-lying electronic states of SiH₂, e.g., \tilde{X}^1A_1 , \tilde{a}^3B_1 and 3A_2 , leading to its predissociation to yield Si (³P). Francisco *et al.*¹³ calculated a substantial barrier height of 44.7 kcal/mol for the dissociation channel from the \tilde{a}^3B_1 state to Si (³P) + H₂, and concluded that the individual rovibronic states of the \tilde{A}^1B_1 state may couple either directly, or via a weakly avoided crossing of the 3A_2 and \tilde{a}^3B_1 surfaces, to the 3A_2 background states and predissociate via this 3A_2 surface to form Si (³P). Direct confirmation for the production of Si atoms following photofragmentation of SiH₂ comes from the studies of Steinfeld and co-workers^{12(c)} (Si ¹D) and Knight and co-workers^{12(e)} (Si ³P).

Our observed results for the \tilde{A}^1B_1 state are summarized as follows:

(1) A radiationless decay channel with strong rotational dependence, opens at $K_a \neq 0$ rotational levels even at the $v_2' = 0$ vibronic level.

(2) In energy region of SiD₂, $v_2' \leq 2$, a radiationless decay channel shows strong deuterium isotope effect, i.e., suppression of the rotational dependent decay channel.

(3) SiH₂, (0,6,0) vibronic level shows different behavior from $v_2' \leq 5$ levels.

(4) A higher energy decay channel occurs in the energy region $v_2' > 7$ for SiH₂ \tilde{A}^1B_1 .

The radiationless decay channel described in case (1) should be predissociation to Si (³P) + H₂ through triplet manifold due to the spin conservation rule. Theoretical calculation⁹ predicted that the 3A_2 state had very different structure from other low-lying electronic states, \tilde{X}^1A_1 , \tilde{A}^1B_1 , and \tilde{a}^3B_1 . Consequently, it is considered that interaction between the 3A_2 and \tilde{A}^1B_1 states is very weak due to

Franck–Condon term in the energy region we are interested in, though these states can directly mix by spin–orbit coupling. On the other hand, the \tilde{A}^1B_1 state cannot directly interact with the \tilde{a}^3B_1 state through spin–orbit coupling. Therefore, we propose a predissociation mechanism with the second order interaction. The decay channel in the higher energy region $v_2' > 7$ is interpreted by opening of the second predissociation channel to Si (¹D) + H₂. The details of the predissociation mechanisms will be discussed in following sections.

C. Rotationally dependent predissociation

As discussed in the previous section, we proposed that the predissociation \tilde{A}^1B_1 to Si (³P) + H₂ is not caused by direct interaction with triplet states, i.e., $\tilde{A}^1B_1 \leftrightarrow \tilde{a}^3B_1$ and $\tilde{A}^1B_1 \leftrightarrow ^3A_2$, but second order interaction. The *a*-type Coriolis interaction between the Renner–Teller pair of the \tilde{A} and \tilde{X} states was observed in absorption spectra.¹ Then, it is considered that the second order interaction is that through the \tilde{X}^1A_1 state, i.e., $\tilde{A}^1B_1 \leftrightarrow \tilde{X}^1A_1 \leftrightarrow \tilde{a}^3B_1$ and/or $\tilde{A}^1B_1 \leftrightarrow \tilde{X}^1A_1 \leftrightarrow ^3A_2$. A substantial barrier height between the \tilde{a}^3B_1 state and dissociation limit, Si (³P) + H₂, was estimated to be 44.7 kcal/mol¹⁷ and, on the other hand, there is little or no barrier between the 3A_2 state and the dissociation limit.⁹ The deuterium isotope effect observed in LIF excitation spectra suggests the existence of a potential barrier in the predissociation channel. Consequently, we conclude that the predissociation occurs by the interaction with the \tilde{a}^3B_1 state, $\tilde{A}^1B_1 \leftrightarrow \tilde{X}^1A_1 \leftrightarrow \tilde{a}^3B_1$. The theoretical calculation⁶ also suggested the strong spin–orbit interaction between the \tilde{X}^1A_1 and \tilde{a}^3B_1 states.

The matrix element of the second order interaction between the \tilde{A}^1B_1 and \tilde{a}^3B_1 states through the \tilde{X}^1A_1 state is given by

$$\begin{aligned} \langle ^1B_1 | H' | ^3B_1 \rangle \\ = - \sum_n \frac{\langle ^1B_1 | H_{or} | ^1A_1(n) \rangle \langle ^1A_1(n) | H_{so} | ^3B_1 \rangle}{(E_s - E_n)(E_t - E_n)}, \quad (3) \end{aligned}$$

where $^1A_1(n)$ is the high vibrational level of \tilde{X}^1A_1 and H_{or} and H_{so} are Hamiltonians of orbital–rotation and spin–orbit interactions, respectively. The *a*-type Coriolis interaction matrix element between \tilde{A}^1B_1 and \tilde{X}^1A_1 is given by²²

$$\langle ^1B_1; J, K | \hat{H}_{or} | ^1A_1; J, K \rangle = -2K_a \langle ^1B_1 | A \hat{L}_a | ^1A_1 \rangle, \quad (4)$$

where A is the rotational constant for rotation around the *a* axis and \hat{L}_a is the orbital angular momentum operator corresponding to the $^1\Delta_g$ state, to which the \tilde{X}^1A_1 and \tilde{A}^1B_1 states correlate in the linear geometry. Petek *et al.*²⁰ reported the same kind of the second order interaction between the \tilde{b}^1B_1 and \tilde{X}^3B_1 states of CH₂. The matrix element is zero at $K_a = 0$ and has nonzero values at $K_a \neq 0$. Time resolved excitation spectra shown in Figs. 3, 4, and 6 are favorably interpreted by this mechanism; the $K_a' = 0$ levels survive in the spectra obtained with late gate times but the $K_a' \neq 0$ levels decay with short lifetimes.

The excitation spectra of SiD₂ show complicated rotational structure in low vibronic levels, $v_2' \leq 2$ as seen in Fig. 5:

The $K'_a \neq 0$ rotational levels are observed for $v'_2 \leq 2$, but only the $K'_a = 0$ levels for $v'_2 \geq 3$. Although the level energy of SiD₂, \tilde{A}^1B_1 ($v'_2 = 2$) is higher than SiH₂, \tilde{A}^1B_1 ($v'_2 = 1$), the spectrum for the (0,2,0)–(0,0,0) band of SiD₂ is much more complex in comparison with that for the (0,1,0)–(0,0,0) band of SiH₂. Considering the predissociation via the second order interaction discussed above, this fact suggests a tunneling mechanism for the predissociation through a potential barrier between \tilde{A}^1B_1 and Si(³P) + H₂. The top of the barrier should lie in energy region between $v'_2 = 2$ and 3, i.e., 1540–2160 cm⁻¹ from the bottom of the \tilde{A}^1B_1 state. The barrier height is lower than that predicted from theoretical calculation,¹³ i.e., 6850 cm⁻¹.

The rotational levels with high J' value in \tilde{A}^1B_1 , (0,6,0) of SiH₂ decay with much longer lifetimes than those in other vibronic levels. Theoretical calculation⁹ predicted that triplet states, ³A₂ and \tilde{a}^3B_1 , intersect at energy of 21.2 kcal/mol above Si(³P) + H₂ dissociation limit, which is comparable to energy difference between Si(³P) and Si(¹D), 18.0 kcal/mol. Accordingly, the anomalous behavior of the $v'_2 = 6$ vibronic level would reflect the interaction of the ³A₂ state with the \tilde{a}^3B_1 state. This anomaly would occur in $v'_2 = 9$ and 10 vibronic states of SiD₂ from energetic consideration, but we could not detect this effect because of low signal intensity.

D. Predissociation from higher vibronic levels of SiH₂ ($v'_2 > 7$)

As mentioned before, a new nonradiative channel appears to open at the $J' = 0$, $K'_a = 0$ levels of SiH₂, \tilde{A}^1B_1 , $v'_2 \geq 7$. This process cannot be attributed to the predissociation caused by the second order interaction discussed above, because the $K'_a = 0$ level predissociates. The \tilde{A}^1B_1 state correlates to Si(¹D) + H₂ in the dissociation limit. We are led to conclude that the homogeneous predissociation to Si(¹D) + H₂ opens between $v'_2 = 6$ and 7 as suggested previously.¹⁴ Steinfeld and co-workers^{12(c)} have confirmed the existence of this nonradiative decay channel through direct detection of Si(¹D) production at $v'_2 = 7$.

The $v'_2 = 10$ level of \tilde{A}^1B_1 SiD₂ lies very close in energy to $v'_2 = 7$ of SiH₂. It is surprising that the decay rate of SiD₂, $v'_2 = 10$ lies just on the straight line in Fig. 10, which means no predissociation occurs from this level. This suggests the existence of a potential barrier, through which hydrogen atoms can pass, on the pathway to dissociation. Francisco *et al.*¹³ measured the fluorescence lifetimes of SiH₂, to be 450 ns for $v'_2 = 7$ and 49 ns for $v'_2 = 8$, and concluded that the shortening of the lifetime at $v'_2 = 8$ was caused by the predissociation opening between $v'_2 = 7$ and 8. The observed lifetime for $v'_2 = 7$, which agrees with our value of 400 ns, is shorter than the radiative lifetime predicted on the basis of our $J' = 0$ measurements (Fig. 11 and discussion above), indicating the existence of decay though a nonradiative process. Their lifetimes can be interpreted satisfactorily with the

tunneling predissociation mechanism: both $v'_2 = 7$ and 8 levels predissociate through the potential barrier.

Finally, we estimate the dissociation limit for Si(³P) + H₂. Using the transition energy for the (0,6,0)–(0,0,0) and (0,7,0)–(0,0,0) bands, the zero point energy of \tilde{X}^1A_1 , and the energy difference between Si(³P) and Si(¹D), the dissociation energy from the potential minimum of the ground state is determined to be 1.88 ± 0.05 eV, which is 0.10 eV lower than the value estimated from *ab initio* calculations by Francisco *et al.*¹³ The heat of formation of SiH₂ is calculated to be ΔH_f^0 (SiH₂) = (2.78 ± 0.09) eV using ΔH_{vap}^0 (Si) = (4.66 ± 0.04) eV.²³

ACKNOWLEDGMENT

This work was supported in part by a Grant-in-Aid on Priority-Area Research on "Photo-Excited Process" supported by Ministry of Education, Science and Culture.

¹I. Dubois, G. Herzberg, and R. D. Verma, *J. Chem. Phys.* **47**, 4262 (1967); I. Dubois, *Can. J. Phys.* **46**, 2485 (1968); I. Dubois, G. Duxbury, and R. N. Dixon, *J. Chem. Soc. Faraday Trans. II* **71**, 799 (1975).

²D. E. Milligan and M. E. Jacox, *J. Chem. Phys.* **52**, 2594 (1970).

³L. Fredin, R. H. Hauge, Z. H. Kafafi, and J. L. Margrave, *J. Chem. Phys.* **82**, 3542 (1985).

⁴B. Wirsam, *Chem. Phys. Lett.* **14**, 214 (1972).

⁵J. H. Meadows and H. F. Schaefer III, *J. Am. Chem. Soc.* **98**, 4383 (1976); M. E. Colvin, R. S. Grev, and H. F. Schaefer III, *Chem. Phys. Lett.* **99**, 399 (1983); W. D. Allen and H. F. Schaefer III, *Chem. Phys.* **108**, 243 (1986).

⁶M. S. Gordon, *Chem. Phys. Lett.* **59**, 410 (1978); S. Koseki and M. S. Gordon, *J. Mol. Spectrosc.* **123**, 392 (1987).

⁷Y. Takahata, *Chem. Phys. Lett.* **59**, 472 (1978).

⁸G. Olbrich, *Chem. Phys. Lett.* **73**, 110 (1980).

⁹J. E. Rice and N. C. Handy, *Chem. Phys. Lett.* **107**, 365 (1984).

¹⁰G. Inoue and M. Suzuki, *Chem. Phys. Lett.* **105**, 641 (1984).

¹¹J. Danon, S. V. Filseth, D. Feldmann, H. Zacharias, C. H. Dugan, and K. H. Welge, *Chem. Phys.* **29**, 345 (1978).

¹²(a) J. W. Thoman, Jr., and J. I. Steinfeld, *Chem. Phys. Lett.* **124**, 35 (1986); (b) J. W. Thoman, Jr., J. I. Steinfeld, R. I. McKay, and A. E. W. Knight, *J. Chem. Phys.* **86**, 5909 (1987); (c) C. W. Van Zoeren, J. W. Thoman, Jr., J. I. Steinfeld, and M. W. Rainbird, *J. Phys. Chem.* **92**, 9 (1988); (d) Y. M. Engel, R. D. Levine, J. W. Thoman, Jr., J. I. Steinfeld, and R. I. McKay, *J. Chem. Phys.* **86**, 6561 (1987); (e) R. I. McKay, A. S. Uichanco, A. J. Bradley, J. R. Holdsworth, J. S. Francisco, J. I. Steinfeld, and A. E. W. Knight, *ibid.* **95**, 1688 (1991).

¹³J. S. Francisco, R. Barnes, and J. W. Thoman, Jr., *J. Chem. Phys.* **88**, 2334 (1988).

¹⁴K. Obi and S. Mayama, *Abstract I-12, International Symposium on Gas Kinetics* (Bordeaux, France, 1986).

¹⁵M. Fukushima and K. Obi, *J. Chem. Phys.* **93**, 8488 (1990).

¹⁶G. Herzberg, *Electronic Spectra of Polyatomic Molecules* (Van Nostrand, New York, 1966).

¹⁷M. Fukushima and K. Obi (unpublished).

¹⁸D. Feldmann, K. Meier, R. Schmiedl, and K. H. Welge, *Chem. Phys. Lett.* **60**, 30 (1978).

¹⁹T. E. Sharp and H. M. Rosenstock, *J. Chem. Phys.* **41**, 3453 (1964).

²⁰H. Petek, D. J. Nesbitt, D. C. Darwin, and C. B. Moore, *J. Chem. Phys.* **86**, 1172 (1987).

²¹D. Husain and P. E. Norris, *J. Chem. Soc. Faraday II* **74**, 1483 (1978).

²²C. G. Stevens and J. D. C. Brand, *J. Chem. Phys.* **58**, 3324 (1973).

²³P. D. Desai, *J. Phys. Chem. Ref. Data* **15**, 967 (1986).